Doubly resonant coherent anti-Stokes Raman spectroscopy of Ce^{3+} in $LuPO_4$

David Piehler and Norman Edelstein
Department of Physics, University of California, Berkeley, California 94720
and Materials and Chemical Sciences Division, Lawrence Berkeley Laboratory, Berkeley, California 94720
(Received 18 December 1989)

We have measured coherent anti-Stokes Raman spectra between crystal-field levels of the $^2F_{5/2}$ and $^2F_{7/2}$ manifolds of the Ce^{3+} ion diluted in $LuPO_4$ at ~ 10 K. The anti-Stokes signal is nearly resonant with the lowest crystal-field level of the $5d^1$ configuration of Ce^{3+} at 30460 cm^{-1}. For a $LuPO_4$ crystal doped with 0.06 mol % Ce^{3+}, we found enhancements of the third-order susceptibility $|\chi^{(3)R}/\chi^{(3)NR}|$ as high as 11.6. This enhancement is over 20 times larger than that seen previously in singly resonant experiments with pure rare-earth crystals.

I. INTRODUCTION

Hougen and Singh[1] first reported Raman scattering between electronic states of rare-earth ions in a crystal in 1963. Unlike electric dipole transitions between crystal-field states of the ground $4f^n$ configuration, which are parity forbidden in first order, Raman transitions between states of the same electronic configuration are parity allowed. The primary use of electronic Raman scattering (ERS) has been to locate and determine the symmetry of low-lying crystal-field levels.[2] The main experimental problem associated with ERS in rare-earth crystals is due to the magnitude of ERS cross sections that are usually much smaller than those encountered in vibrational Raman scattering. For example, the total Raman cross section of the 992-cm^{-1} vibrational mode in benzene[3] is 2.7×10^{-28} cm^2, while electronic Raman cross sections for rare-earth ions in crystals[4,5] range from 5×10^{-29} to 1×10^{-33} cm^2. Crystals with dilute concentrations of rare-earth ions will have even smaller *effective* cross sections. If the energies of the electronic levels are close to the optical phonons of the crystal, the phonon Raman signal may overwhelm the ERS signal. In addition, electronic linewidths increase rapidly with temperature, necessitating the use of a cryogenic cooling system for the crystals.

For these reasons, coherent electronic Raman spectroscopy in rare-earth crystals[6,7] has shown only limited success unlike coherent vibrational Raman spectroscopy.[8,9] The intensity of the signal from coherent anti-Stokes Raman spectroscopy (CARS) is proportional to the square of the third-order electronic susceptibility $|\chi^{(3)}|^2$. The quantity $\chi^{(3)}$ is the sum of a nonresonant part that is due to the bulk crystal, and a resonant, frequency-dependent part that contains the spectroscopic information,

$$\chi^{(3)}=\chi^{(3)NR}+\chi^{(3)R} . \quad (1)$$

Since $\chi^{(3)R}$ is roughly proportional to the spontaneous Raman cross section, we have

$$|\chi^{(3)R}_{el}| < |\chi^{(3)R}_{vib}| . \quad (2)$$

The resonant susceptibility for electronic CARS, $\chi^{(3)R}_{el}$, is often so small that is it obscured by $\chi^{(3)NR}$, which can be orders of magnitude larger. This is especially true for dilute rare-earth crystals, since $\chi^{(3)R}_{el}$ is proportional to the number density of rare-earth ions in the crystal.

Experiments[10–17] have shown that ERS cross sections in rare-earth crystals can be resonantly enhanced when the frequency of the exciting laser is near the energy of an electronic level of the rare-earth ion. These studies included inter- and intraconfigurational resonances. In the case of intraconfigurational resonant ERS, the intermediate state is within the same electronic configuration as the initial and final state, i.e., $4f^n$ for the rare-earth ions. The ERS cross sections involve electric dipole-matrix elements between the initial and final states to the intermediate states. Electric dipole $4f^n\rightarrow4f^n$ transitions are parity forbidden in first order, but the odd components of the crystal-field mix excited states of opposite parity (such as the $4f^{n-1}5d^1$) with the $4f^n$ crystal-field states to allow relatively weak second-order "forced electric dipole" transitions. Interconfigurational resonant ERS directly use excited states of opposite parity ($4f^{n-1}5d^1$), and the enhancement of the ERS signal is much stronger. For most trivalent rare-earth ions, these excited configurations have energies greater than 50000 cm^{-1}, and are inaccessible to conventional spectroscopic sources.

Studies of ERS in very dilute crystals involve interconfigurational resonances. Keil and Scott[10] observed ERS between levels of the ground $4f^15d^1$ configuration of 10^{-3} mol % Ce^{2+} in CaF_2 crystals. They used a laser in resonance with the excited $4f^2$ configuration. Piehler, Kot, and Edelstein[18] detected ERS between crystal-field levels of the $5f^1$ configuration of ~0.1 mol % Pa^{4+} in Cs_2ZrCl_6 crystals using a laser 525 cm^{-1} below the lowest level of the $6d^1$ configuration.

Among the trivalent rare-earth ions, the Ce^{3+} ion with its single $4f$ electron is not only the simplest ion to analyze, but also has the lowest energy $4f^{n-1}5d^1$ configuration. In the solid state, the onset of the $5d^1$ configuration varies from 22000 cm^{-1} for Ce^{3+}:YAG (Ref. 19) (where YAG is yttrium aluminum garnet) to 40000 cm^{-1} for Ce^{3+}:LaF_3.[20] In Ce^{3+}:$LuPO_4$, the

 ©1990 The American Physical Society

lowest crystal-field level of the $5d^1$ configuration begins at 30 460 cm^{-1}.

Williams *et al.*[16,17] took advantage of the relatively low energy of the $5d^1$ configuration in a 0.6 mol% Ce^{3+}:$LuPO_4$ crystal and measured ERS intensities between the ground state and excited crystal-field states of the $^2F_{5/2}$ and $^2F_{7/2}$ manifolds. They performed this experiment with lasers at 354.7 nm (28 192 cm^{-1}) and 514.5 nm (19 430 cm^{-1}). A change of laser source from 514.5 to 354.7 nm resulted in the enhancement of the ERS intensity by a factor an order of magnitude larger than could be accounted for by the ω^4 dependence of the Raman cross section.

In this paper, we report on electronic CARS experiments on a 0.06 mol% Ce^{3+}:$LuPO_4$ crystal. By using a frequency tripled Nd^{3+}:YAG laser (28 192 cm^{-1}) and a tunable dye laser operating in the 26 000-cm^{-1} range, we satisfy two resonance conditions. When the difference in energy between the two lasers is equal to the energy of the lower crystal-field levels of the $^2F_{7/2}$ manifold, the CARS signal will be in the 30 400-cm^{-1} range, less than 100 cm^{-1} below the lowest $5d^1$ band. (See Fig. 1.) With this extra resonance we find that the resonant susceptibility is large enough to compete with $\chi^{(3)NR}$, even in a dilute crystal.

There have been many degenerate wave-mixing experiments in rare-earth crystals, but relatively few experimenters have reported wave mixing with lasers of two or more colors as in this work. The work of Shand[6] and Traar[7] involved singly resonant CARS in pure rare-earth crystals and will be discussed in Sec. III. Cone and coworkers have measured multiresonant two-photon absorption induced four-wave mixing in $Tb(OH)_3$, $LiTbF_4$, and TbF_3 crystals.[21–24] Recently, Mosharay *et al.* observed three-level photon echoes in Pr^{3+}:LaF_3.[25]

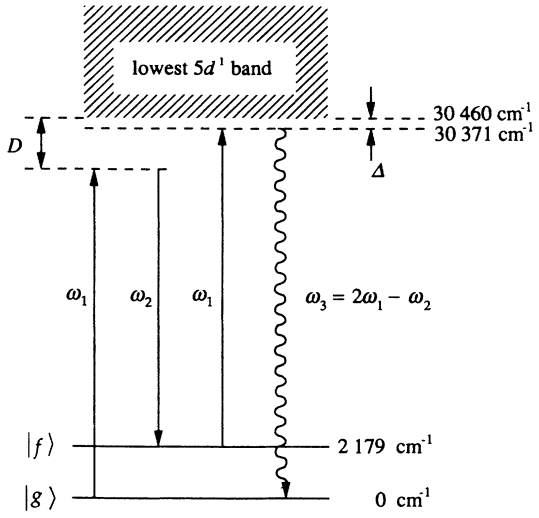

FIG. 1. Schematic diagram of doubly resonant CARS in Ce^{3+}:$LuPO_4$. $\omega_1/2\pi c = 28\,192$ cm^{-1}, $\omega_2/2\pi c = 26\,013$ cm^{-1}, $(2\omega_1-\omega_2)/2\pi c = 30\,371$ cm^{-1}, $\Delta = 89$ cm^{-1}, and $D = 2268$ cm^{-1}.

II. ELECTRONIC STRUCTURE OF Ce^{3+}:$LuPO_4$

Early experiments by Hoshina and Kuboniwa[26] and Nakazawa and Shinoya[27] measured the electronic structure of Ce^{3+} in $LuPO_4$ from $5d^1 \leftrightarrow 4f^1$ emission and excitation spectra. More recently, Williams *et al.*[16,17,28] made a detailed examination of the ground $4f^1$ configuration by electronic Raman scattering and the excited $5d^1$ configuration by absorption measurements. Their results are shown in Fig. 2.

The host crystal $LuPO_4$ is an insulator with a band gap of about 70 000 cm^{-1}.[29] It is uniaxial with the tetragonal zircon structure (space group D_{4h}^{19}).[30] We define the z axis as parallel to the highest symmetry crystal axis. The Ce^{3+} ions substitute for the Lu^{3+} ions at sites of D_{2d} symmetry. Since the Ce^{3+} ion has an odd number (one) of optically active electrons, the crystal-field levels are labeled by the irreducible representations of the double group of D_{2d}, Γ_6 and Γ_7. Each crystal-field level is a Kramers doublet.

The spin-orbit interaction splits the lowest-energy configuration $4f^1$ into two multiplets $^2F_{7/2}$ and $^2F_{5/2}$ separated by about 2200 cm^{-1}. The crystal field further splits the $4f^1$ configuration into a total of seven crystal-field states as shown in Fig. 2.

The energy-level structure of the first excited configuration $5d^1$ of the Ce^{3+} ion in $LuPO_4$ is significantly different from that of the $4f^1$ configuration. The radial wave function of the $5d^1$ electron extends farther beyond the filled $5s^25p^6$ shells of the Xe core which results in a much stronger interaction between the $5d^1$ electron and the crystal lattice. In the $4f^1 \rightarrow 5d^1$ absorption spectrum, this increased strength manifests itself in three ways. First, the crystal field is now stronger than

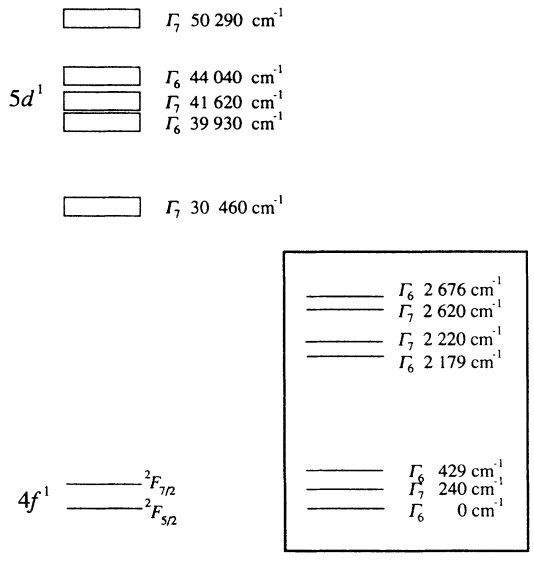

FIG. 2. Energy-level diagram for Ce^{3+}:$LuPO_4$. All levels are labeled by irreducible representations of the double group of D_{2d}. Energy values and symmetry labels on the $5d^1$ levels refer to the zero-phonon lines. An expanded view of the $4f^1$ crystal-field levels is shown in the box at right.

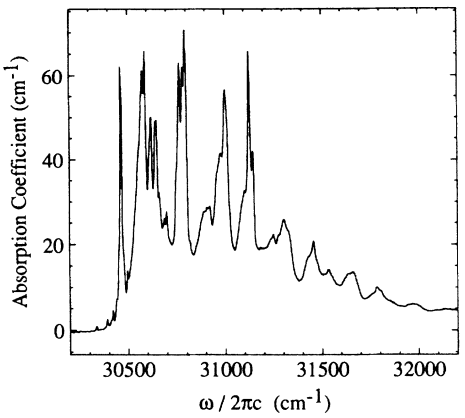

FIG. 3. Low-temperature absorption spectra of the lowest $5d^1$ band. The small peaks to the left of the zero-phonon line are due to absorption from populated vibrational levels.

the spin-orbit coupling. The crystal-field and the spin-orbit interactions split the $5d^1$ configuration into five crystal-field levels which have energies from 30 000 to 50 000 cm^{-1}. (See Fig. 2.) Furthermore, the absorption spectrum of each of these levels may be characterized by a zero-phonon line and a broad vibronic sideband. (See Fig. 3.) The zero-phonon line corresponds to a purely electronic transition between the ground state and the $5d^1$ level. The vibronic sideband, which lies on the higher energy side of the zero-phonon line, results from the stronger coupling between the $5d^1$ electronic state and the vibrational states of the host crystal. Since inhomogeneous strain broadening is directly related to the strength of the crystal field, inhomogeneous broadening for the $5d^1$ levels is an order of magnitude larger than for the $4f^1$ configuration.

III. THEORY

A. Singly resonant CARS

The resonant third-order suceptibility tensor governing singly resonant CARS [shown schematically in Fig. 4(a)] is[31]

$$\chi^{(3)\mathrm{R}}_{ijkl}(-\omega_3,\omega_1,\omega_1,-\omega_2) = \frac{-N\Lambda}{12\hbar}\sum_f \frac{\alpha_{ij}(\omega_3,\omega_1)\alpha_{kl}(\omega_1,\omega_2)}{(\omega_1-\omega_2-\omega_{gf}-i\Gamma_{gf})}\ , \tag{3}$$

where

$$\alpha_{uv}(\omega_x,\omega_y)=\frac{1}{\hbar}\sum_n \left[\frac{\langle g|er_u|n\rangle\langle n|er_v|f\rangle}{(\omega_x-\omega_{gn})} - \frac{\langle g|er_v|n\rangle\langle n|er_u|f\rangle}{(\omega_y+\omega_{gn})}\right] \tag{4}$$

is the usual (nonresonant) Raman tensor. The quantities ω_1, ω_2, and ω_3 are the frequencies of the input lasers and the output signal, respectively. The indices i, j, k, and l denote the polarizations of the ω_3, ω_1, ω_1 and ω_2 beams, respectively. The kets $|g\rangle$, $|f\rangle$, and $|n\rangle$ correspond to the ground, low-lying, and intermediate states with energies zero, $\hbar\omega_{gf}$, and $\hbar\omega_{gn}$. The number density of scatterers is N, and Γ_{gf} is the linewidth [half width at half maximum (HWHM)] of the $|g\rangle\rightarrow|f\rangle$ transition. The term $\Lambda=[(n^2+2)/3]^4$, where n is the refractive index, contains the local field corrections.

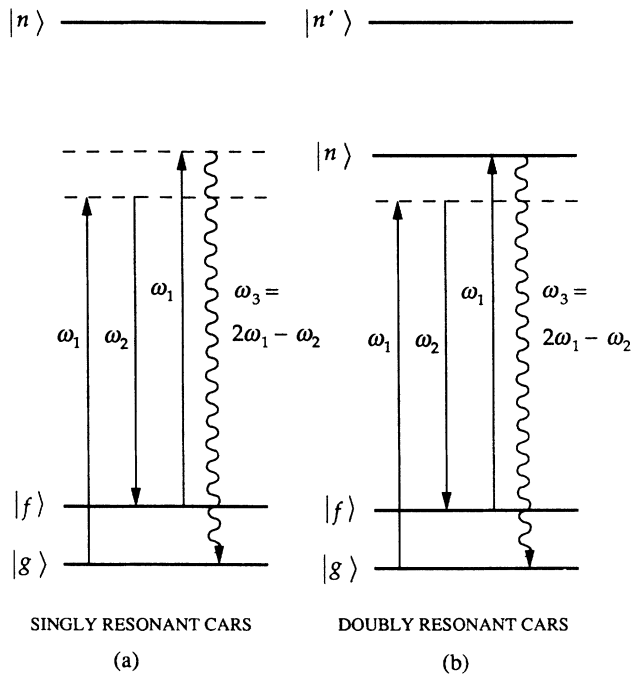

FIG. 4. Schematic diagram of singly and doubly resonant CARS. The dashed lines are not real states, and are drawn to aid the eye.

The CARS signal I_3, at $\omega_3=2\omega_1-\omega_2$ is proportional to the square of the total third-order susceptibility tensor

$$I_3 \propto |\chi^{(3)\mathrm{NR}}+\chi^{(3)\mathrm{R}}|^2\ , \tag{5}$$

where for simplicity we have suppressed the tensor indices. If we consider only a single low-lying level $|f\rangle$ and note that the Raman tensors are essentially independent of ω_1 and ω_2 as $\omega_1-\omega_2$ is swept through ω_{gf}, we may write Eq. (3) as

$$\frac{\chi^{(3)\mathrm{R}}}{\chi^{(3)\mathrm{NR}}}=\frac{A}{(\delta-i\Gamma)}\ , \tag{6}$$

where $\delta=\omega_1-\omega_2-\omega_{gf}$. The intensity of the CARS signal normalized to the off-resonance intensity is

$$\frac{I_3}{I_3^{\mathrm{NR}}}=\frac{|\chi^{(3)\mathrm{R}}+\chi^{(3)\mathrm{NR}}|^2}{|\chi^{(3)\mathrm{NR}}|^2}=1+\frac{2A\delta}{\delta^2+\Gamma^2}+\frac{A^2}{\delta^2+\Gamma^2}\ . \tag{7}$$

At $\delta=0$, $|\chi^{(3)\mathrm{R}}/\chi^{(3)\mathrm{NR}}|$ reaches a maximum value of A/Γ. In order to observe the resonance against the background, the quantity $C=|\chi^{(3)\mathrm{R}}/\chi^{(3)\mathrm{NR}}|_{\max}=A/\Gamma$ should be greater than the experimental noise-to-signal ratio. We may consider C to be a figure of merit for CARS experiments. Systems with larger values of C yield better information.

According to Eqs. (3) and (4), when the laser frequencies are far below the intermediate states, $|\chi^{(3)R}|$ takes a maximum value

$$|\chi^{(3)R}|_{max}=\frac{N\Lambda|\alpha|^2}{12\hbar\Gamma} . \quad (8)$$

The Raman tensor is related to the total Raman cross section σ by

$$\sigma=\frac{8\pi\Lambda\omega_s^4|\alpha|^2}{3c^4} . \quad (9)$$

For a typical pure rare-earth crystal, $N\approx10^{22}$ cm^{-3}, $\Gamma/2\pi c\approx2$ cm^{-1}, and the intermediate states of opposite parity lie above 50 000 cm^{-1}. A typical Stokes frequency is $\omega_s/2\pi c\approx20\,000$ cm^{-1}. Using the above cited figures for ERS cross sections, we find that $|\chi^{(3)R}|_{max}$ for singly resonant electronic CARS should vary between 5×10^{-14} and 1×10^{-18} esu. For a dilute rare-earth crystal such as the crystal discussed in this paper, $N\approx10^{19}$ cm^{-3} and $\Gamma/2\pi c\approx0.2$ cm^{-1}. This implies that $|\chi^{(3)R}|_{max}$ will vary from 5×10^{-16} to 1×10^{-20} esu. For most transparent solids $\chi^{(3)NR}\approx10^{-14}$ esu,[32] and $|\chi^{(3)R}|_{max}$ will be the same order of magnitude or smaller than $\chi^{(3)NR}$. We conclude that in singly resonant CARS, the enhancement of $\chi^{(3)}$ due to resonances between electronic states of rare-earth ions will be modest at best. For dilute rare-earth crystals, $C\ll1$, and detection of singly resonant CARS will be difficult, if not impossible.

Experiments by Shand[6] and Traar[7] are consistent with this conclusion. Both selected favorable rare-earth systems to obtain the highest values of C. Shand measured electronic CARS resonances between the crystal-field levels of ground $^7F_6$ manifold and the $^7F_5$ manifold of the Tb^{3+} ion in $Tb_3Al_5O_{12}$ at 80 K, and found $C\leq0.4$. Traar investigated electronic CARS resonances from the $^3H_4\leftrightarrow{}^3F_2$ transition of Pr^{3+} in PrF_3 at 2 K, and found $C\leq0.5$.

B. Doubly resonant CARS

For doubly resonant CARS, the resonant third-order susceptibility tensor corresponding to Fig. 4(b) is[31]

$$\chi^{(3)R}_{ijkl}(-\omega_3,\omega_1,\omega_1,-\omega_2)=\frac{-N\Lambda}{12\hbar^3}\sum_f\frac{1}{(\omega_1-\omega_2-\omega_{gf}-i\Gamma_{gf})}\times\sum_n\frac{\langle g|er_i|n\rangle\langle n|er_j|f\rangle}{(\omega_3-\omega_{gn}-i\Gamma_{gn})}\times\sum_{n'}\frac{\langle g|er_k|n'\rangle\langle n'|er_l|f\rangle}{(\omega_1-\omega_{gn'})} . \quad (10)$$

In the above equation, both summations n and n' are over *all* intermediate states. Double resonance is a route by which $\chi^{(3)R}$ may be increased to compete favorably with $\chi^{(3)NR}$. Equation (10) indicates that $|\chi^{(3)R}|_{max}$ will increase as $\hbar\omega_3$ and $\hbar\omega_1$ approach the energies of the intermediate states $\hbar\omega_{gn}$ and $\hbar\omega_{gn'}$. For this reason, we chose to work with a crystal containing Ce^{3+} ions whose $5d^1$ configuration lies in the near ultraviolet. Using the 514.5-nm line of an argon-ion laser (19 430 cm^{-1}), Williams *et al.* measured absolute values for the ERS cross sections between the ground-state and the crystal-field levels of the $^2F_{7/2}$ manifold.[28] These ranged from $(0.14-2.5)\times10^{-29}$ cm^2 which are on the high end of the range of rare-earth ERS cross sections. The low-lying $5d^1$ configuration in Ce^{3+}:$LuPO_4$ accounted for its large spontaneous ERS cross section. Using the methods of the previous section, we estimate that for singly resonant CARS in dilute Ce^{3+}:$LuPO_4$, $|\chi^{(3)R}|_{max}\approx2.5\times10^{-16}$ esu.

The lowest $5d^1$ band in Ce^{3+}:$LuPO_4$ begins at 30 460 cm^{-1}. (See Fig. 3.) By using the frequency-tripled output of a Nd^{3+}:YAG laser (28 192 cm^{-1}) and a tunable light source in the 26 000-cm^{-1} region, a CARS resonance between the ground state and the lowest level of the $^2F_{7/2}$ manifold at 2179 cm^{-1} produces a signal at $\omega_3/2\pi c=30\,371$ cm^{-1}. (See Fig. 1.) If we assume that the lowest $5d^1$ level is most important for the Raman cross section, we can estimate the enhancement of $\chi^{(3)R}$ relative to its singly resonant value (i.e., at $\omega_1/2\pi c=19\,430$ cm^{-1}). According to Eq. (10),

$$|\chi^{(3)R}|_{max}\propto\frac{1}{\Gamma_{gf}}\sum_n\frac{1}{(\omega_3-\omega_{gn})}\sum_{n'}\frac{1}{(\omega_1-\omega_{gn'})} , \quad (11)$$

if $|\omega_3-\omega_{gn}|\gg\Gamma_{gn}$. Since the entire lowest $5d^1$ band contributes, we replace the summations in the above equation by integrals weighted by the absorption data of Fig. 3. Numerical integration gives an enhancement factor of about 97. Now $|\chi^{(3)R}|_{max}$ may be as great as 2.5×10^{-14} esu for the dilute Ce^{3+}:$LuPO_4$ crystal. By going from single to double resonance we have gone from $C\ll1$ to $C\geq1$. This is the primary point of this paper.

C. Selection rules

The symmetry of the crystal-field levels imposes selection rules on the tensor $\chi^{(3)R}_{ijkl}$ which are that of the product of Raman tensors $\alpha_{ij}\cdot\alpha_{kl}$. In our experiment, all polarizations are parallel so that we are interested in $\chi^{(3)R}_{iiii}$. For electronic CARS resonances $|g\rangle\leftrightarrow|f\rangle$ the following selection rules apply:

$\Gamma_6\leftrightarrow\Gamma_6$ $\chi^{(3)R}_{iiii}$ allowed for $i=x,y,z$

$\Gamma_6\leftrightarrow\Gamma_7$ $\chi^{(3)R}_{iiii}$ allowed for $i=x,y$ $(\chi^{(3)R}_{zzzz}=0)$.

IV. EXPERIMENT

The Ce^{3+}:$LuPO_4$ crystal was grown as described previously.[29] X-ray fluorescence analysis indicated that 0.0604 mol % of Lu^{3+} have been replaced by Ce^{3+}, and the number density of Ce^{3+} ions is 8.71×10^{18} cm^{-3}. The sample size is $1\times2\times5$ mm^3 with the laser light passing through 1 mm of material. Since the natural crystal faces are of good optical quality, they were left unpolished. The crystal was mounted in a Janis Supertran Cryostat, and cooled to about 10 K. The sample could be oriented

such that the z axis was either parallel or perpendicular to the polarization of the input beams ω_1 and ω_2. This facilitated measurement of $\chi^{(3)R}_{xxxx}$ and $\chi^{(3)R}_{zzzz}$. Since the crystal is uniaxial $\chi^{(3)R}_{xxxx}=\chi^{(3)R}_{yyyy}$.

The frequency tripled light from a Spectra-Physics DCR-1 Nd^{3+}:YAG laser at $\omega_1/2\pi c=28\,191.5$ cm^{-1} provided one beam, and also pumped a dye laser to provide tunable radiation in the $\omega_2/2\pi c\approx 26\,000$-$cm^{-1}$ range. The polarization of both beams were parallel. A 25-cm focal length lens focused both beams onto a 100-μm spot on the sample. Optimal phase matching was achieved when the angle between the two beams was 48 mrad. The linewidths for ω_1 and ω_2 were 0.8 and 0.6 cm^{-1} [full width at half maximum (FWHM)], respectively. The energy per pulse was 200 μJ for each beam, and the duration of ω_1 was 10 ns, and ω_2 was 5 ns. The Nd^{3+}:YAG laser was operated at a 10-Hz repetition rate, and the optical configuration was adjusted to give the maximum temporal overalp of ω_1 and ω_2 at the sample.

A SPEX 1403 double momochromator analyzed the CARS signal at $\omega_3=2\omega_1-\omega_2$, and an RCA 1P28A photomultiplier tube detected the signal. The bandwidth of the monochromator was about 10 cm^{-1}. In addition, a biased silicon photodiode (EG&G SGD-100A) detected attenuated light from beam ω_2. A pair of Stanford Research Systems SR250 boxcar integrators measured the pulses from both the photomultiplier and the photodiode.

A personal computer collected individual measurements of the CARS signal, normalized this signal to ω_2 for each laser shot, and averaged these values over 75 laser shots. After collecting each set of data, the computer scanned the dye laser to a new value of ω_2 and adjusted the monochromator to maintain the relationship $\omega_{\text{monochromator}}=2\omega_1-\omega_2$.

The nature of the lowest $5d^1$ band is of primary importance to this work. In order to measure the lowest $5d^1$ band, a 60-W D_2 lamp illuminated the sample and the transmitted light was directed into the double monochromator which operated in second order because it cannot scan beyond 31 000 cm^{-1} in first order. The intensity of light as a function of frequency yielded the absorption spectrum of the first $5d^1$ band as shown in Fig. 3. The instrumental resolution was about 2 cm^{-1}. The x and z polarized spectra were nearly identical.

Figure 3 shows small peaks to the left of the zero-phonon line. At higher resolution, the spectrum showed that these peaks have counterparts to the right of the zero-phonon line, with which they form symmetric pairs about the zero-phonon line. We conclude that the peaks on the left are due to absorption from populated vibrational levels of the ground electronic state. The mechanism for population may be from the $5d^1\rightarrow 4f^1$ fluorescence excited by the D_2 lamp or from the radiation of the D_2 lamp heating the crystal. No absorption losses were seen in the CARS signal when the CARS output frequency matched these peaks. Since the CARS process does not change the quantum state of the system, there is no mechanism by which the vibrational levels may be populated.

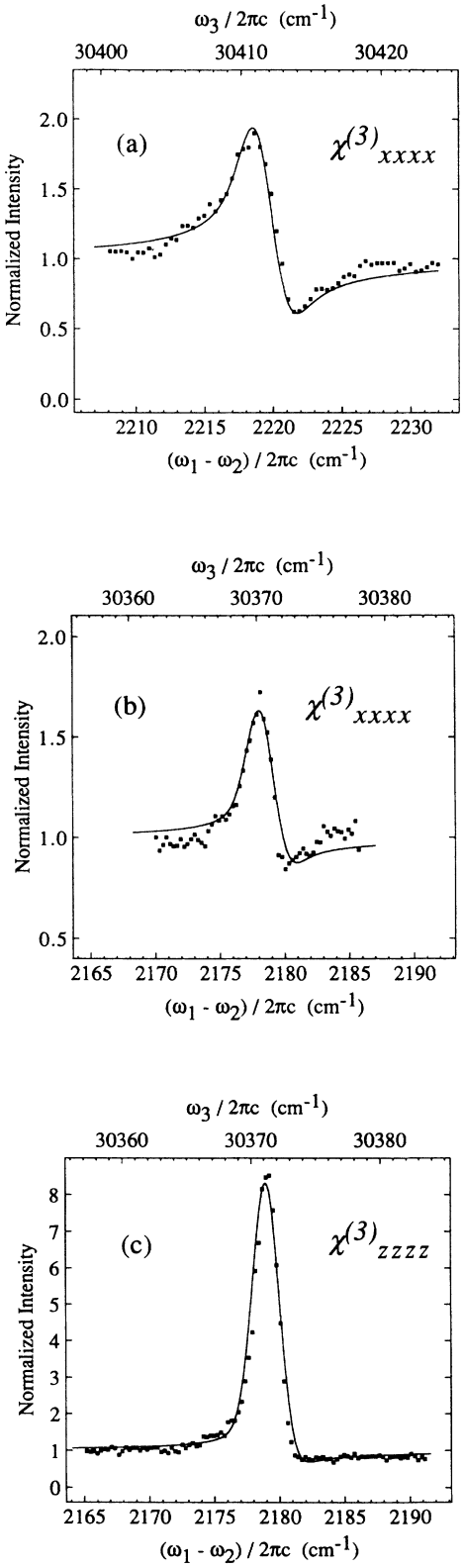

FIG. 5. Intensity of CARS signal at frequency ω_3 as a function of $\omega_1-\omega_2$ normalized to the off-resonance intensity. The solid line is a fitted curve with the parameters listed in Table I. (a) and (b) show $|\chi^{(3)}_{xxxx}/\chi^{(3)NR}_{xxxx}|^2$ while (c) shows $|\chi^{(3)}_{zzzz}/\chi^{(3)NR}_{zzzz}|^2$. No enhancement of $\chi^{(3)}_{zzzz}$ was seen in the $(\omega_1-\omega_2)/2\pi c\approx 2220$-$cm^{-1}$ region.

V. RESULTS AND ANALYSIS

A. Data

We have measured enhancements in the third-order susceptibility due to electronic transitions between the ground Γ_6 state and the two lower levels of the $^2F_{7/2}$ manifold at 2179 cm^{-1} (Γ_6) and 2220 cm^{-1} (Γ_7). We did not observe the two upper levels of the $^2F_{7/2}$ manifold because the CARS signals from these two levels are within the $5d^1$ absorption band. Figure 5 shows the intensities of the signals normalized to the off-resonance intensities as a function of frequency and polarization. As expected from the selection rules, we observed no resonance between the Γ_6 ground state and the Γ_7 level at 2220 cm^{-1} in the z polarization.

B. Calculation of $\chi^{(3)R}$

In order to fit the observed spectra, the form of $\chi^{(3)R}$ as a function of ω_1, ω_2, and ω_3 must be known. We assume the same form $\chi^{(3)R}/\chi^{(3)NR}=A/(\delta-i\Gamma)$ [Eq. (6)] as used for singly resonant CARS with a single low-lying level. Since this is a doubly resonant experiment with a number of Raman active electronic levels, we must justify this choice with respect to Eq. (10).

The two lowest crystal-field levels of the $^2F_{7/2}$ manifold are separated by 41 cm^{-1}. Since this separation is much greater than the linewidths of either level, we may treat these levels separately, and the susceptibilities for each level will not interfere with each other.

In a doubly resonant CARS experiment,[33] the line shape of the signal changes as ω_3 moves through resonance with the intermediate state $|n\rangle$. In terms of Eq. (10) this occurs for two reasons. First, $i\Gamma_{gn}$ may become comparable in magnitude to $(\omega_3-\omega_{gn})$ adding an additional phase to $\chi^{(3)R}$. In addition, the quantity $(\omega_3-\omega_{gn})$ may vary considerably throughout the spectrum, shifting both the magnitude and phase of $\chi^{(3)R}$. For the conditions of the experiment reported here, both of these effects are small and may be safely ignored as demonstrated below.

All $5d^1$ bands (zero-phonon lines and vibronic sidebands) act as intermediate states for the CARS process, and we must sum over the entire $5d^1$ configuration in Eq. (10). If the coupling between the Ce^{3+} ion and the host lattice is not too strong, the intermediate states may be described by the Born-Oppenheimer approximation, and written as the product

$$|n\rangle=|n_e\rangle|\chi_v\rangle\ , \tag{12}$$

where $|n\rangle$ labels the nth $5d^1$ band ($n=1-5$), $|n_e\rangle$ labels the nth electronic state of the Ce^{3+}-ion $5d^1$ configuration, and $|\chi_v\rangle$ labels the vibrational state of the crystal. Then

$$\omega_{gn}=\omega^e_{gn}+\omega_\chi\ , \tag{13}$$

where $\hbar\omega^e_{gn}$ is the energy of the nth zero-phonon line (purely electronic transition), and $\hbar\omega_\chi$ corresponds to the phonon states. The crystal-field levels of the $4f^1$ configuration involved in the CARS experiment have the same vibrational quantum number, namely $|0_v\rangle$. We may write

$$\langle g|er_i|n\rangle\langle n|er_i|f\rangle=\langle g_e|er_i|n_e\rangle\langle n_e|er_i|f_e\rangle|\langle\chi_v|0_v\rangle|^2. \tag{14}$$

If ω_1 is far enough below the $5d^1$ bands, the following approximation holds for the final summation in Eq. (10):

$$\sum_{n'}\frac{\langle g|er_i|n'\rangle\langle n'|er_i|f\rangle}{(\omega_1-\omega_{gn'})} \propto \sum_{\text{all } 5d^1 \text{ bands}}\frac{\langle g_e|er_i|n'_e\rangle\langle n'_e|er_i|f_e\rangle}{(\omega_1-\bar{\omega}_{gn'})}\ , \tag{15}$$

where $\bar{\omega}_{gn'}$ are the centers of gravity of the five $5d^1$ bands. Since we are interested in $\chi^{(3)}_{iiii}$, all tensor indices are the same.

For the second summation in Eq. (10), only the lowest $5d^1$ band contributes appreciably. The absorption coefficient a for the ground state to the lowest $5d^1$ level is

$$a(\omega_{gn})\propto|\langle g_e|er_i|1_e\rangle|^2|\langle 0_v|\chi_v\rangle|^2\ . \tag{16}$$

The intensity of the absorption spectrum of the lowest $5d^1$ band shows very little polarization behavior. Hence $|\langle g_e|er_i|1_e\rangle|^2$ may be treated as a constant, independent of i. Then Eqs. (14) and (16) allow the following change to be made to the second summation in Eq. (10):

$$\sum_n\frac{\langle g|er_i|n\rangle\langle n|er_i|f\rangle}{(\omega_3-\omega_{gn}-i\Gamma_{gn})}\propto\langle g_e|er_i|1_e\rangle\langle 1_e|er_i|f_e\rangle \times\int_{\text{first } 5d^1 \text{ band}}\frac{a(\omega_{gn})}{(\omega_3-\omega_{gn})}d\omega_{gn}\ . \tag{17}$$

Note that we have disregarded the $i\Gamma_{gn}$ term. This is justified in our experiment because $|\omega_3-\omega_{gn}|/2\pi c$ is always ≥ 50 cm^{-1}, which is much larger than $\Gamma_{gn}/2\pi c$ for the individual levels which make up the $5d^1$ band.

Now Eq. (10) may be written as

$$\chi^{(3)R}_{iiii}\propto\frac{1}{\delta-i\Gamma}\langle g_e|er_i|1_e\rangle\langle 1_e|er_i|f_e\rangle\int_{\text{first } 5d^1 \text{ band}}\frac{a(\omega_{gn})}{(\omega_3-\omega_{gn})}d\omega_{gn}\sum_{\text{all } 5d^1 \text{ bands}}\frac{\langle g_e|er_i|n'_e\rangle\langle n'_e|er_i|f_e\rangle}{(\omega_1-\bar{\omega}_{gn'})}\ . \tag{18}$$

The frequency-tripled Nd^{3+}:YAG laser provides ω_1, which is a constant. The absorption coefficient $a(\omega_{gn})$ is plotted in Fig. 3. Numerical evaluation of the integral in Eq. (18) shows that its value changes only slightly as ω_3 varies throughout each resonance. The value of the integral varies by only 1% over the line profiles in Figs. 5(b) and 5(c) and by about 5% over Fig. 5(c). For this reason, we treat the integral as a constant over each resonance.

We therefore fit our data to

$$\frac{\chi^{(3)R}_{iiii}}{\chi^{(3)NR}_{iiii}} = \frac{A}{(\delta - i\Gamma)} . \tag{19}$$

We have directly measured $\chi^{(3)NR}_{xxxx}/\chi^{(3)NR}_{zzzz} = 1.48 \pm 0.15$ in a pure $LuPO_4$ crystal which allows us to compare all observed resonances. Williams *et al.*[17] have calculated angular wave functions for all electronic levels of the $4f^1$ and $5d^1$ configurations. Using the absorption data of Fig. 3, relative values of A may be calculated according to Eq. (18) and compared with experiment. Since the features to the left of the zero-phonon line in Fig. 3 are not connected to the ground state, we did not include them in the calculation. The basis of the calculations rests on the assumption that the $5d^1$ states may be described by the Born-Oppenheimer approximation. The Born-Oppenheimer approximation does not, however, affect our choice of Eq. (19) as an appropriate functional form for $\chi^{(3)R}$.

C. Deconvolution of the spectra

Ideally, one would like to fit the data of Fig. 5 to Eq. (7). However, the actual spectra must be deconvolved, in order to take into account the finite bandwidths of the input lasers. The output intensity is written as[34]

$$I(\omega_3) \propto \int |\chi^{(3)}|^2 g_1(\omega_1) g_1(\omega_3 + \omega_1 - \omega_2) g_2(\omega_2) d\omega_1 d\omega_2 , \tag{20}$$

where $g_i(\omega)$ is the normalized intensity of beam ω_i centered at ω_i^0. Since the input lasers have finite linewidths, the output $I(\omega_3)$ will have a frequency distribution centered at $\omega_3^0 = 2\omega_1^0 - \omega_2^0$. The detector bandwidth is greater than that of $I(\omega_3)$ so the data correspond to

$$I(\omega_3^0 = 2\omega_1^0 - \omega_2^0) \propto \int I(\omega_3) d\omega_3 . \tag{21}$$

Our lasers have approximately Gaussian line shapes with FWHM 0.8 cm^{-1} for ω_1 and 0.6 cm^{-1} for ω_2. These measurements were made with the double monochromator with slits closed to a point where the bandwidth ≈ 0.25 cm^{-1}. The accuracy of the laser linewidth measurements is ± 0.1 cm^{-1}. With Gaussian intensity profiles for the input lasers, the above equations cannot be evaluated in closed form. The CARS signals in Fig. 5 may be fit by numerically computing $I(\omega_3^0)$. A least-squares fit is obtained by treating A and Γ as variable parameters. Table I summarizes these results. The fitted curves are drawn as solid lines in Fig. 5. The major effect of using lasers with linewidths greater than the crystal linewidths is a general broadening of the spectra, especially when $\Delta\omega_{laser} > 2\Gamma$. Perhaps most noticeable is the suppression of the "dip" in the CARS signal in Figs. 5(b) and 5(c). Here the normalized intensity does not fall far below 1 as in a typical CARS intensity profile. In Fig. 5(a), $\Delta\omega_{laser} < 2\Gamma$, and the effect is minimal.

D. Analysis

Although the above analysis strictly applies only to homogeneously broadened lines, we view Γ as a phenomenological parameter which may include contributions from both homogeneous and inhomogeneous broadening. The ability to accurately measure these quantities is hampered by using broadband lasers. The third column of Table I lists the linewidths for the various levels. The linewidth of the lower crystal-field level is much narrower than the higher level. This is expected since the higher level may decay by the spontaneous emission of a phonon. The Debye energy of the $LuPO_4$ crystal is 300 cm^{-1},[35] making nonradiative decay from the 2179-cm^{-1} level to the 429-cm^{-1} level relatively slow. As a consequence, the 2220-cm^{-1} state is lifetime broadened, while the linewidth of the 2179-cm^{-1} level may be primarily attributed to crystal strain broadening. These measured linewidths are typical of those found in dilute rare-earth crystals at low temperatures.[36]

The fourth column of Table I gives the value of C for the different resonances. The bandwidths and noise levels of the lasers place limits on how weak a resonance we can detect. For a resonance with $\Gamma/2\pi c = 0.045$ cm^{-1}, our lower limit of detection is $C < 0.5$. For a resonance with $\Gamma/2\pi c = 0.45$ cm^{-1}, our lower limit of detection is $C < 0.05$. When we preformed this experiment with visible lasers ($\omega_1/2\pi c = 18\,792$ cm^{-1}, $\omega_2/2\pi c \approx 16\,600$ cm^{-1}), we observed no CARS resonances. Therefore, by going from singly to doubly resonant CARS, we observed an increase in C by *at least* a factor of 23.

The fifth and sixth columns of Table I give experimental and calculated values of A. The calculated values are normalized to the experimental value of A for the x-polarized 2179-cm^{-1} resonance. Agreement between the experiment and the calculation is fair.

The use of broadband lasers masks the true size of the resonance for narrow lines. Had we used lasers with

TABLE I. Summary of data with estimated uncertainties. $C = |\chi^{(3)R}_{iii}/\chi^{(3)NR}_{iii}|_{max} = A/\Gamma$. $\chi^{(3)NR}_{xxxx}/\chi^{(3)NR}_{zzzz} = 1.48 \pm 0.15$. The calculated values of A are normalized to the experimental value of A for the x-polarized 2179-cm^{-1} resonance.

i	$\omega/2\pi c$ (cm^{-1})	$\Gamma/2\pi c$ (HWHM) (cm^{-1})	C	$A/2\pi c$ (experimental) (cm^{-1})	$A/2\pi c$ (calculated) (cm^{-1})
z	2179	0.045 ± 0.015	11.6 ± 0.5	0.52 ± 0.15	1.25
z	2220		< 0.05	< 0.03	0
x	2179	0.049 ± 0.015	3.1 ± 0.1	0.15 ± 0.04	0.15
x	2220	0.45 ± 0.10	1.2 ± 0.1	0.55 ± 0.10	0.83

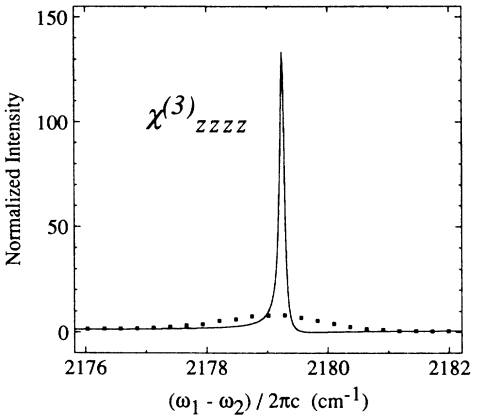

FIG. 6. Calculated CARS signal using the data of Table I, and assuming input lasers have zero linewidth. For comparison, the data of Fig. 5(c) are also shown.

sub-gigahertz bandwidths, the signal peak in Fig. 5(c) would be about 130 times as large as the off resonance intensity. Figure 6 shows the data of Fig. 5(c) along with the CARS signal calculated from Eq. (7) (which neglects the finite laser linewidths) using the parameters in Table I. The use of broadband lasers has a small effect on the 2220-cm^{-1} resonance.

E. Summary

We have demonstrated doubly resonant CARS between electronic states in a dilute rare-earth crystal. The signals produced are an order of magnitude larger than those seen previously in singly resonant CARS in pure rare-earth crystals. Two factors account for the large values of $C = |\chi^{(3)R}/\chi^{(3)NR}|_{max}$. First and most important is the enhancement due to the signal being in near resonance with the lowest $5d^1$ band. In addition, the narrow linewidth of the lowest level of the $^2F_{7/2}$ manifold gives C an extra boost.

The use of doubly resonant CARS should be applicable to high-resolution spectroscopy of other dilute rare-earth systems. Requirements are, in order of importance, accessible $5d$ levels, electronic transitions with narrow linewidths, and lasers with bandwidths narrower than the material resonances. Crystals doped with divalent rare-earth ions are attractive candidates. The $5d$ bands of divalent rare-earth ions are in the visible and near infrared. At low temperatures electronic linewidths of dilute crystals are ultimately limited by inhomogeneous broadening. Dilute single crystals usually have inhomogeneous broadening (FWHM) in the 1–10-GHz range.[36] Finally, in order to accurately measure the resonance, and to avoid deconvolution of spectra, narrow band lasers should be employed.

ACKNOWLEDGMENTS

L. A. Boatner and M. M. Abraham of Oak Ridge National Laboratory generously supplied the crystals used in this work. We acknowledge helpful discussions with Sumner Davis, Glen Williams, and Paolo Foggi. This research was supported in part by the Director, Office of Energy Research, Office of Basic Energy Sciences, Chemical Sciences Division of the U.S. Department of Energy under Contract No. DE-AC03-76SF00098.

[1]J. T. Hougen and S. Singh, Phys. Rev. Lett. **10**, 406 (1963).
[2]R. J. H. Clark and T. J. Dines, in *Advances in Infrared and Raman Spectroscopy*, edited by R. J. H. Clark and R. E. Hester (Heyden, London, 1982), Vol. 9, p. 282.
[3]Y. Kato and H. Takuma, J. Chem. Phys. **54**, 5398 (1971).
[4]A. Kiel and S. P. S. Porto, J. Mol. Spectrosc. **32**, 458 (1969).
[5]J. A. Koningstein and O. Sonnich Mortensen, Phys. Rev. **168**, 75 (1968).
[6]M. L. Shand, J. Appl. Phys. **52**, 1470 (1981).
[7]K. P. Traar, Phys. Rev. B **35**, 3111 (1987).
[8]*Chemical Applications of Nonlinear Raman Spectroscopy*, edited by A. B. Harvey (Academic, New York, 1981).
[9]*Advances in Non-linear Spectroscopy*, edited by R. J. H. Clark and R. E. Hester (Wiley, Chichester, 1988).
[10]A. Kiel and J. F. Scott, Phys. Rev. B **2**, 2033 (1971).
[11]R. L. Wadsack and R. K. Chang, Solid State Commun. **10**, 45 (1972).
[12]D. Nicollin and J. A. Koningstein, Chem. Phys. **49**, 377 (1980).
[13]P. Myslynski and J. A. Koningstein, Chem. Phys. **114**, 137 (1987).
[14]Philippe C. Becker, Ph.D. thesis, University of California, Berkeley, 1986.
[15]P. C. Becker, G. M. Williams, R. E. Russo, N. Edelstein, J. A. Koningstein, L. A. Boatner, and M. M. Abraham, Opt. Lett. **11**, 282 (1986).
[16]Glen M. Williams, Ph.D. thesis, Univeristy of California, Berkeley, 1988.
[17]G. M. Williams, P. C. Becker, J. G. Conway, N. Edelstein, L. A. Boatner, and M. M. Abraham, Phys. Rev. B **40**, 4132 (1989).
[18]D. Piehler, W. Kot, and N. Edelstein (unpublished).
[19]G. Blasse and A. Brill, Appl. Phys. Lett. **11**, 53 (1967).
[20]L. R. Elias, W. S. Heaps, and W. M. Yen, Phys. Rev. B **8**, 4989 (1973).
[21]R. L. Cone, D. A. Ender, M. S. Otteson, P. L. Fisher, J. M. Freidman, and H. J. Guggenheim, in *Laser Techniques for Extreme Ultraviolet Spectroscopy, Subseries on Optical Science and Engineering Number 2*, Proceedings of the Topical Meeting on Laser Techniques for Extreme Ultraviolet Spectroscopy, AIP Conf. Proc. No. 90, edited by T. J. McIlrath and R. R. Freeman (AIP, New York, 1982), p. 471.
[22]R. L. Cone, D. A. Ender, M. S. Otteson, P. L. Fisher, J. M. Freidman, and H. J. Guggenheim, Appl. Phys. B **28**, 143 (1982).
[23]D. A. Ender, M. S. Otteson, R. L. Cone, and H. J. Guggenheim, Opt. Lett. **7**, 611 (1982).
[24]J. Huang, B. Jaquier, and R. L. Cone (unpublished).
[25]F. Mosharay, R. Kichinski, R. J. Beach, and S. R. Hartmann, Phys. Rev. A **40**, 4426 (1989).
[26]T. Hoshina and S. Kuboniwa, J. Phys. Soc. Jpn. **31**, 828 (1971).

[27]E. Nakazawa and S. Shionoya, J. Phys. Soc. Jpn. **36**, 504 (1974).

[28]G. M. Williams, N. Edelstein, L. A. Boatner, and M. M. Abraham, Phys. Rev. B **40**, 4143 (1989).

[29]W. O. Milligan, D. F. Mullica, G. W. Beall, and L. A. Boatner, Inorg. Chim. Acta **60**, 39 (1982).

[30]E. Nakazawa and F. Shiga, J. Lumin. **15**, 255 (1977).

[31]Y. R. Shen, *The Principles of Nonlinear Optics* (Wiley, New York, 1984). The factor of 12 is added to conform to the notation of P. D. Maker and R. W. Tehrune, Phys. Rev. **137**, A801 (1965).

[32]M. D. Levenson and N. Bloembergen, Phys. Rev. B **10**, 4447 (1974).

[33]R. T. Lynch, H. Lotem, and N. Bloembergen, J. Chem. Phys. **66**, 4250 (1977).

[34]M. A. Yuratich, Mol. Phys. **38**, 625 (1979).

[35]A. Armbruster, R. Thomä, and H. Wehrle, Phys. Status Solidi A **24**, K71 (1974).

[36]R. M. Macfarlane, in *Lasers, Spectroscopy, and New Ideas,* edited by W. M. Yen and M. D. Levenson (Springer-Verlag, New York, 1988), p. 205.